Ultra-thin Free-Standing Oxide Membranes for Electron and Photon Spectroscopy Studies of Solid-gas and Solid-liquid Interfaces

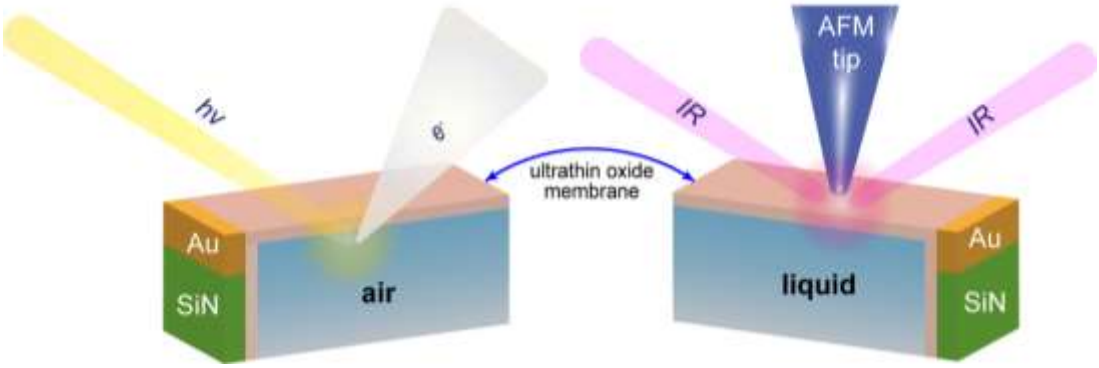

Yi-Hsien Lu [†,#], Carlos Morales [†,‡,#], Xiao Zhao [†,§,#], Matthijs A. van Spronsen [†], Artem Baskin [∥], David Prendergast [∥], Peidong Yang [†,Δ], Hans Bechtel [⊥], Edward Barnard [∥], Frank Ogletree [∥], Virginia Altoe [∥], Leonardo Soriano [‡], Adam Schwartzberg [∥] and Miquel Salmeron [†,§,]*

[†] Materials Sciences Division, Lawrence Berkeley National Laboratory, Berkeley, California, 94720, United States

[∥] Molecular Foundry, Lawrence Berkeley National Laboratory, Berkeley, California, 94720, United States

[§] Department of Materials Science and Engineering, University of California at Berkeley, Berkeley, California 94720, United States

[Δ] Department of Chemistry, University of California, Berkeley, California, 94720, United States

[⊥] Advanced Light Source, Lawrence Berkeley National Laboratory, Berkeley, California, 94720, United States

[‡] Departamento de Física Aplicada and Instituto de Ciencia de Materiales Nicolás Cabrera, Universidad Autónoma de Madrid, Francisco Tomás y Valiente 7, 28049 Madrid, Spain

ABSTRACT

Free-standing ultra-thin (~2 nm) films of several oxides (Al_2O_3, TiO_2, and others) have been developed, which are mechanically robust and transparent to electrons with $E_{kin} \geq 200$ eV, and to photons. We demonstrate their applicability in environmental X-ray photoelectron and infrared spectroscopy for molecular level studies of solid-gas (≥1 bar) and solid-liquid interfaces. These films act both as membranes closing a reaction cell, and as substrates and electrodes for electrochemical reactions. The remarkable properties of such ultra-thin oxides membranes enable atomic/molecular level studies of interfacial phenomena, such as corrosion, catalysis, electrochemical reactions, energy storage, geochemistry, and biology, in a broad range of environmental conditions.

KEYWORDS: oxide membranes, electrochemistry, operando spectroscopy, XPS, nano-FTIR.

TEXT

Metal and semiconductor oxides are some of the most abundant materials on Earth and their interactions with aqueous solutions and atmospheric gases are at the base of corrosion, geochemical, catalytic, and electrochemical processes[1-3]. In industry, metal oxides play a crucial role in applications ranging from heterogeneous catalysis, photocatalysis, energy storage, fuel cells, and chemical sensors[4-7]. Therefore, the ability to characterize the metal oxide interface with gases and liquids at the atomic/molecular scale is essential for understanding these processes. Over the past decades, various surface sensitive techniques have been developed toward this goal. These include electron and X-ray based spectroscopies, such as X-ray photoelectron

spectroscopy (XPS), electron-yield X-ray absorption spectroscopy (EY-XAS), Auger electron spectroscopy (AES), scanning electron microscopy (SEM), and transmission electron microscopy (TEM), which provide structural and elemental identification of species at surfaces/interfaces[8]. However, the current pressure range where these techniques operate is still lower than that needed in many practical reaction conditions, and their operation in liquid environments remains particularly difficult. To extend the pressure range and to enable measurements in the liquid phase, thin film membranes acting as windows in environmental cells have been developed recently. Micro fabricated thin silicon nitride films (5-200 nm) supported on Si chips are the most popular ones and can be used as window materials for the separation of high vacuum and gases or liquid at ambient pressures[9, 10]. Si, SiO_2, thin carbon films, and graphene have also been used as thin film window materials for this purpose[11-14]. In particular, graphene has extraordinary mechanical strength and can sustain large pressure differences while being impermeable to gases and liquids[15, 16]. The atomic-scale thickness of graphene makes it sufficiently transparent to electrons and for this reason it has been used in a variety of environmental cells for electron-based microscopies and spectroscopies, such as TEM, SEM, AES and XPS[14, 17-21]. Recently, graphene membranes were also applied in infrared (IR) nanospectroscopy (nano-FTIR) studies of the molecular structure of liquids near graphene[22].

Here we present a new generation of ultra-thin (few nm) membranes based on oxide materials. These ultra-thin oxides have remarkable mechanical strength and can withstand large pressure differences, which makes them useful as cell membrane windows. Like graphene, as we will show, they are transparent to photons, and to electrons with a wide range of kinetic energies. The membranes can be used as supports of metal particles for catalysis studies, as electrodes in electrocatalysis, in batteries, and in many other applications.

Fabrication and chemical composition of the metal oxide films

Figure 1(a) shows a schematic representation of the fabrication process. We start with commercial silicon nitride membranes, abbreviated as SiN, perforated with holes of 500-2000 nm diameter. We coat these membranes with gold (or other metals), Figure 1(a) step i, and subsequently cover them with a graphene layer on the flat side (Figure 1(a) step ii). The purpose of gold is to improve adhesion and to ensure good electrical connectivity between graphene domains. The oxide film is grown by plasma enhanced atomic layer deposition (PE-ALD)[23-27] on either side of the graphene[23-25], as illustrated in Figure 1(a) step iii-a and iii-b. The graphene can be removed, if desired, by oxygen plasma to leave only the suspended metal oxide (step iv in Figure 1(a)). Typically, however, we keep the graphene on the external side of the window as it adds mechanical strength and because it provides good electrical conductivity for biasing the metal oxide when acting as an electrode. Figure 1(b) shows an atomic-force microscopy (AFM) topographic image of a region of the SiN with holes capped with graphene, while 1(c) is an image of the same area with a 2 nm TiO_2 film grown on the flat side, showing its excellent conformal distribution. Figure 1(d) shows a region of an Al_2O_3-covered array of holes which were initially covered by a Formvar polymer (polyvinyl formal). The polymer acts as support for the PE-ALD growth and was subsequently dissolved in chloroform so that the metal oxide membrane is freely suspended. The details about PE-ALD growth and transfer process can be found in the Supporting Information. The local thickness of metal-oxides was estimated by electron energy-loss spectroscopy (EELS) using the log-ratio method (Figure S2)[28]. Other measurements using AFM and Ellipsometry are described in the SI.

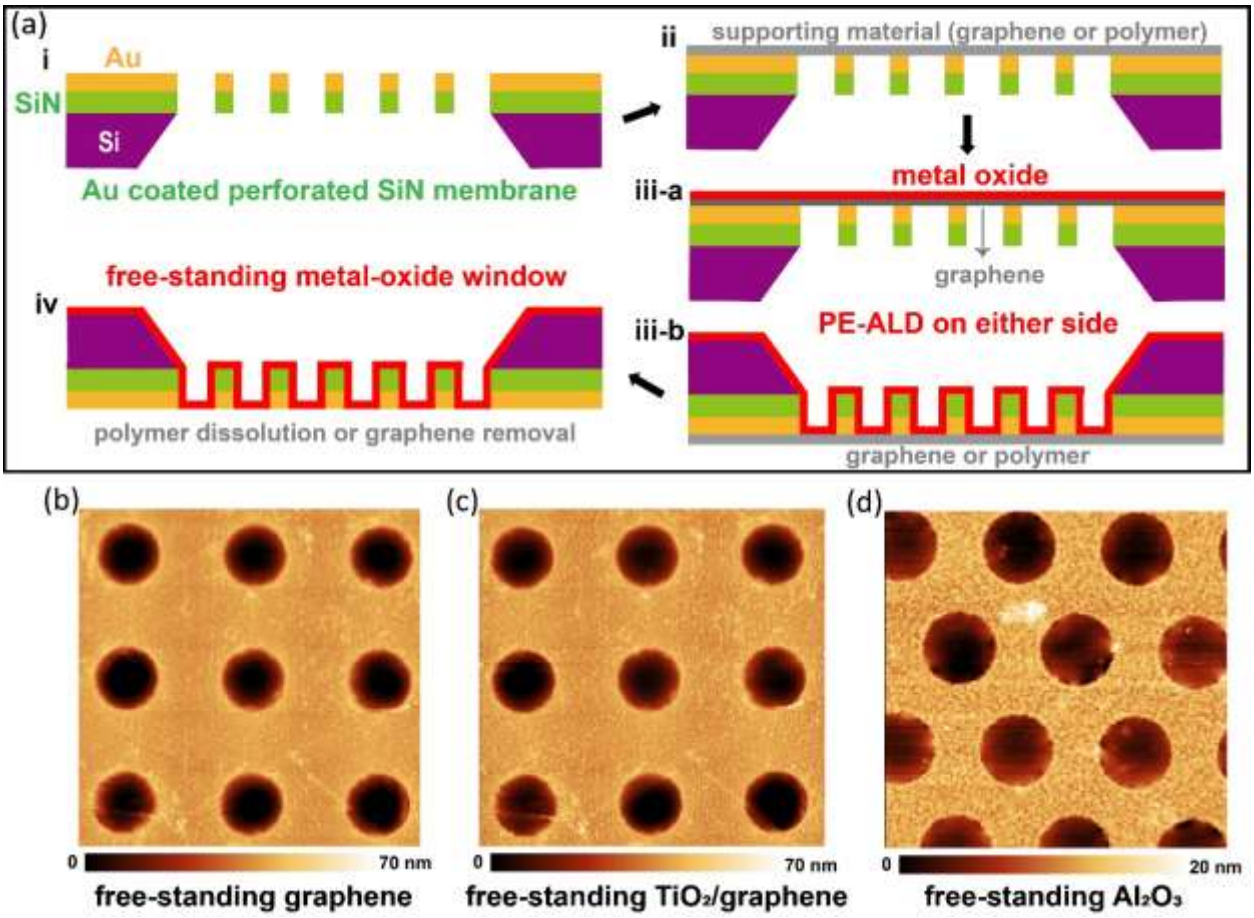

Figure 1 (a) Fabrication process of the free-standing ultra-thin metal oxide membranes. The flat side is exposed to the environment outside the cell, while the corrugated side faces the interior of the cell. (b) AFM topographic image showing a region with a graphene-capped array of holes (ϕ = 1 μm), corresponding to step ii. (c) After deposition of a TiO_2 film (red line) on the flat side of the graphene showing the uniformity of film (step iii-a) (d) AFM topographic image showing a region with a 2 nm thick Al_2O_3 film covering the holes (ϕ = 500 nm, step iv). In this case, Formvar (polyvinyl formal) polymer was used as a support for the PE-ALD process on the corrugated side and dissolved afterwards, leaving the Al_2O_3 film suspended.

The chemical composition and uniformity of the films were examined by scanning Auger spectroscopy (with spatial resolution of few nm), and by TEM/EELS. As shown in Figure 2(a), when TiO_2 is deposited on the side facing the cell interior (corresponding to the SEM image in Figure 2(b)), the Ti LMM Auger peaks only appear when the electron beam is focused on the free-standing graphene/TiO_2 (magenta) but not on the region between holes (blue). Because of the short inelastic mean free path of the 380-eV Auger electrons (around 1 nm), the spectra shows only Ti peaks on the suspended graphene region of the membrane. Figure 2(c) shows a

TEM image of a region of a SiN with a hole partly covered by a free-standing graphene/TiO_2 membrane (the missing part of the membrane is the brightest part). Figure 2d shows a map of the Ti-$L_{2,3}$ loss peak intensity (EELS) from the region marked by a square that includes the ruptured edge. The smoothness of the contrast over the film, and its abrupt change across the edge demonstrates the chemical uniformity of the metal oxide layer over the free-standing graphene. An electron-diffraction pattern from the graphene/TiO_2 area is shown in Figure 2(e). Only the hexagonal diffraction pattern from graphene can be seen since the amorphous metal oxide does not produce diffracted beams. This is expected from the low-temperature (40-120°C) metal oxide deposition conditions[23-26, 29]. Similar results were obtained for Al_2O_3/graphene membranes (Figure S3).

At the temperature used in the PE-ALD growth process a high content of carbon (around 15%) was observed by XPS as a residue of the organic precursor. Surface OH^- groups could also bring out an excess of oxygen[30, 31]. In a separate test, a 20 nm thick Al_2O_3 layer was grown on a SiN wafer to study in more detail its chemical composition and the possibility of cleaning the surface OH^- groups without altering the structural quality of the ultra-thin membranes. Figure S4 shows an XPS depth profile measurement and how the initial element concentrations of the uppermost layer converges to the stoichiometric 3/2::O/Al ratio in the bulk. The profile also shows that the carbon content drops to less than a 2% in the Al_2O_3 bulk. The carbon and OH^- groups can be eliminated by a gentle sputtering with Ar_{75}^+ clusters at low energy (8000 eV) without discernible damage on the ultra-thin film deposits (Table S1)[32].

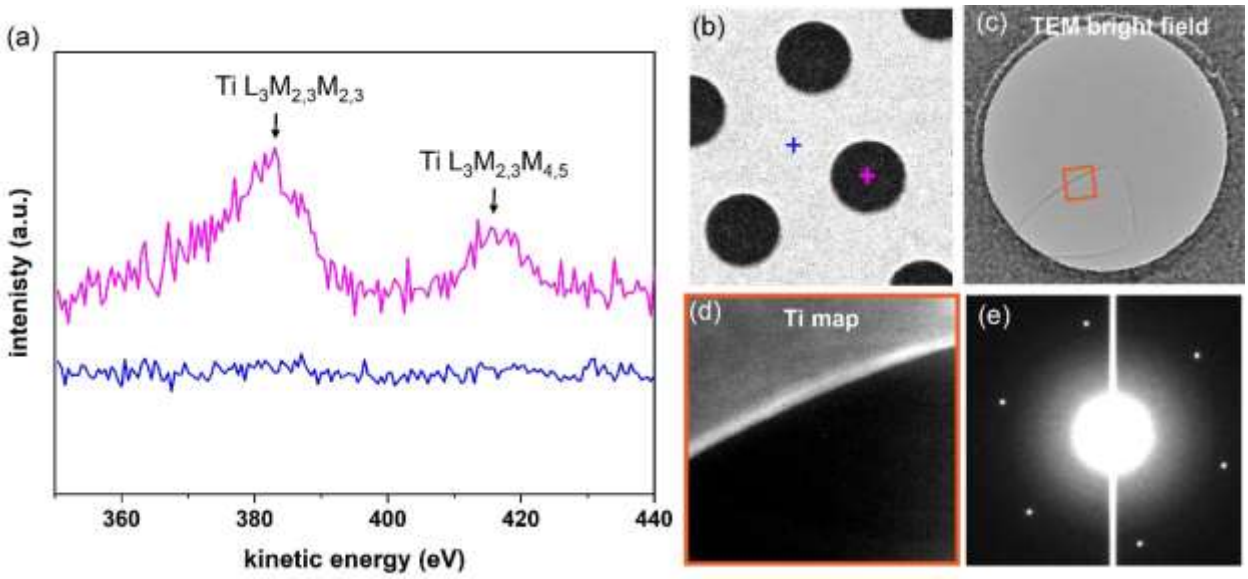

Figure 2 (a) High spatial resolution (few nm) Auger spectroscopy on the graphene/Au/SiN region (blue), and on the free-standing graphene/TiO_2 window (magenta). (b) SEM image showing marks at the location where the Auger spectra were taken. (c) TEM bright field image from a partially ruptured graphene/TiO_2 window (ϕ = 1000 nm). (d) EELS (Ti-L edge) map from the region marked by a square in (c) containing the edge of the ruptured. (e) Electron diffraction pattern from a TiO_2/graphene region showing the hexagonal pattern from graphene, with the amorphous TiO_2 contributing only to the background.

Mechanical properties of metal oxide films

The mechanical behavior of the free-standing metal oxide membranes was investigated by nano-indentation using an AFM tip. To check for indentation-induced damage to the tip, AFM topographic images were acquired before and after each indentation. Figure 3 shows representative force-distance curves on a 1-μm-diameter hole covered with a suspended graphene membrane without (blue) and with (black) a 2-nm-thick TiO_2 film deposited on the membrane facing the cell interior. Details of the AFM nano-indentation can be found in the Methods section. Only a small difference is visible between the loading and unloading curves in both cases, suggesting an elastic deformation process and no sliding between the graphene and TiO_2 layers during indentation, indicative of strong adhesion between graphene and TiO_2. The effective Young's modulus (E) of the suspended membrane was calculated using equation (1)[15,

[24, 25], which describes the force vs indentation depth of a suspended clamped circular sheet of a isotropic elastic material under a centrally applied load,

$$F = \left[3\frac{4\pi E}{1-\nu^2}\left(\frac{t^3}{a^2}\right)\right]\delta + (\pi T)\delta + \left(\frac{q^3 E t}{a^2}\right)\delta^3 \qquad (1),$$

where t = thickness of the suspended membrane, ν = effective Poisson's ratio, a = radius of the suspended membrane, T = pre-tension in the suspended membrane, q is a dimensionless parameter equal to $1/(1.05 - 0.15\nu - 0.16\nu^2)$, F = applied force, and δ = indentation depth. By using Equation (1) and fitting the force-indentation curves, shown as green and red curves corresponding to graphene and graphene/TiO_2, respectively, in Figure 3, we obtain the Young's modulus of graphene, $E_{graphene}$, to be around 404 ± 14 GPa and that of the 2-nm-thick TiO_2 film on graphene, $E_{graphene/TiO2}$, to be 200 ± 100 GPa. These values are close to the values reported in the literature.[24, 25] The $E_{graphene}$ value, however, is lower than that reported for graphene prepared by mechanical exfoliation of graphite (~1 TPa),[15] which could be due to defects in the graphene used in this study stemming from the chemical vapor deposition process and/or from the transfer processes. Assuming a tip radius between 10 and 50 nm, we estimate that our free-standing metal oxide membrane can withstand local pressures higher than 10^6 Pa, i.e, more than 10 bar, which explains its good performance as an environmental cell window to contain high pressure gas or liquids.

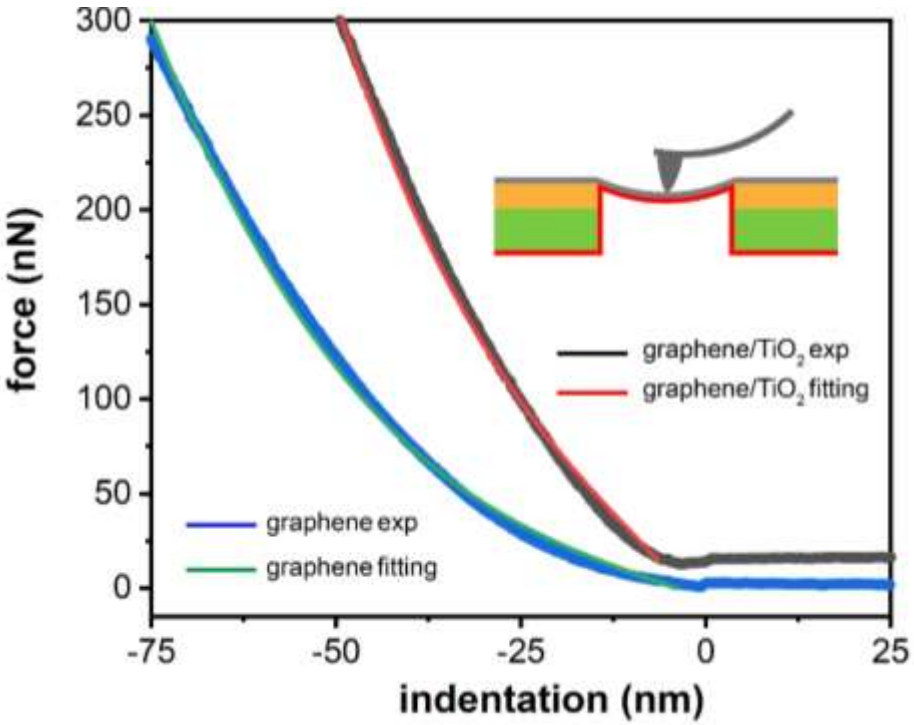

Figure 3 AFM nanoindentation curves of a suspended graphene (blue) and graphene/TiO_2 (black). The green and red curves correspond to the fitting results of graphene and graphene/TiO_2, respectively, using Equation (1). The inset shows a schematic of the AFM nanoindentation experiment.

Metal oxide membranes for electron spectroscopy studies of solid-gas interfaces

The sub-micrometer thickness of SiN membranes (and other materials) makes them transparent to high-energy radiation, in particular ≥100 keV electrons and X-rays, and for that reason they are frequently used for TEM[9, 33] and X-rays absorption spectroscopies in fluorescent-yield detection mode (FY-XAS)[34, 35]. Other surface sensitive spectroscopies such as XPS and EY-XAS which use emitted electrons traversing the membrane are not possible with standard SiN membranes because of the short mean free path of a few nm of low-energy electrons in solid materials. However, the ultra-thin metal oxide films presented above make possible XPS measurements of species present near the membrane, similar to the case of graphene[21]. Figure 4(a) and 4(b) shows the N1s and O1s photoelectron spectra from air at 1 bar enclosed by a 2-nm-

thin Al_2O_3 free-standing membrane. The cell is located inside a vacuum chamber with 10^{-6}-10^{-7} Torr base pressure containing an XPS spectrometer. In Figure 4(a), The N1s spectrum shows a sharp peak at a binding energy of ~405 eV from the N_2 gas phase, together with a small contribution at ~400 eV from N in the SiN support[21]. Similarly, in Figure 4(b), the O1s spectrum shows a doublet peak (due to paramagnetic splitting) at ~537-540 eV corresponding to the O_2 gas phase[36, 37] and another peak at 532.5 eV from the O in the Al_2O_3 membrane. The integrated intensity ratio of the N_2 to O_2 peaks is close to 4, as expected from the air composition.

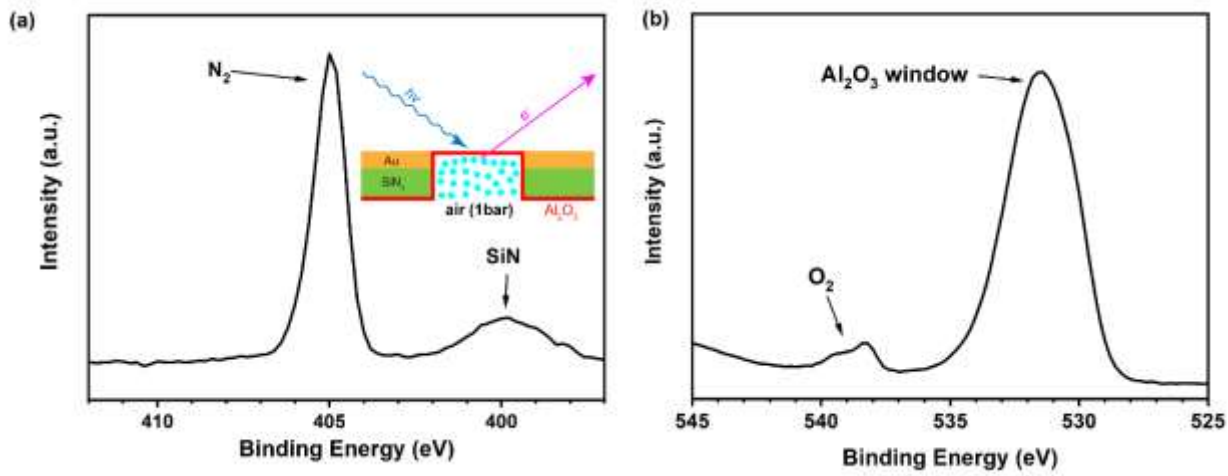

Figure 4 XPS measurements through a 2-nm-thick Al_2O_3 membrane closing a cell filled with 1 bar of air. The cell is located inside an XPS vacuum chamber with a 10^{-6} to 10^{-7} Torr background pressure. (a) N1s spectra, containing a sharp peak from N_2 gas in air and a smaller peak from the SiN support. (b) O1s peak showing the doublet peak from O_2 gas in air and a strong, broad peak from the Al_2O_3 oxide. The photon energy is 1135 eV.

Infrared spectroscopy studies at the interface between metal oxide and liquid.

Vibration spectroscopies based on photons, such as Fourier-transform infrared spectroscopy (FTIR), Raman spectroscopy, and sum-frequency generation spectroscopy (SFG) are powerful and noninvasive tools for studies of surfaces and interfaces[38-41]. Most materials, specially insulating metal oxides, are highly transparent to visible and infrared light and thus they allow

for easy access to the buried solid-liquid interface. The lack of spatial resolution, particularly in the IR case, can be overcome by taking advantage of the plasmonic enhancement in confined geometries and near the corners of sharp objects[42-44]. We recently demonstrated this using an AFM tip to achieve nanoscale resolution FTIR spectra through a graphene membrane electrode to determine the nature of the species in their vicinity (i.e., in the electrical double layer) and their variation with applied bias[22]. Here we demonstrate that this is also possible with our ultra-thin graphene/metal oxide membranes. Figure 5(a) shows the schematic of the nano-FTIR measurement through the graphene/TiO_2 window of a liquid in the cell. Figure 5(b) is the AFM topographic image of a region containing a graphene/TiO_2 (3 nm thick) window in contact with a 0.1M sodium sulfate aqueous solution. The corresponding amplitude of the scattered IR at the second harmonic of the tip oscillation is shown in Figure 5(c). The amplitude over the graphene/TiO_2 window (dark color) is much smaller than that over the graphene−gold region (gold color), as expected from the negligible absorption of graphene−gold compared to the poorly reflective graphene/TiO_2 window. The nano-FTIR spectrum of a 0.1 M sodium sulfate solution in contact with the TiO_2 of the graphene/TiO_2 membrane at open circuit condition (averaged from spectra acquired over many points in the membrane), is shown at the bottom of Figure 5(d). For comparison, the attenuated total reflection FTIR (ATR-FTIR) from a 0.1M droplet of aqueous sodium sulfate solution is shown at the top in Figure 5(d). As can be seen, the expected peaks from the antisymmetric S=O stretching mode in SO_4^{2-} (around 1100 cm^{-1}) and from the bending mode of water (~ 1650 cm^{-1}) are visible in both cases. However, the sulfate-to-water-peak ratio in nano-FTIR is much larger than that of the ATR-FTIR measurements, the former reflecting the near surface region (nm), while the later reflects the bulk (μm) composition of the solution[22]. Several additional peaks between 1200 cm^{-1} and 1600 cm^{-1} are also present in

the nano-FTIR whose nature is still under investigation[45, 46]. Interestingly, while in the case of a pure graphene membrane in contact with 0.1M ammonium sulfate solution, the sulfate peak is about 4 times more intense than that of water,[22] the ratio near the TiO_2 film is about 2 or less. These results indicate that the structure of the electrolyte in the electrical double layer is highly influenced by the nature of the electrode and by the additional hydrogen-bonding of water with O in the metal oxide surface, which provides an anchoring and orienting mechanism for water, very different from that in the hydrophobic graphene.

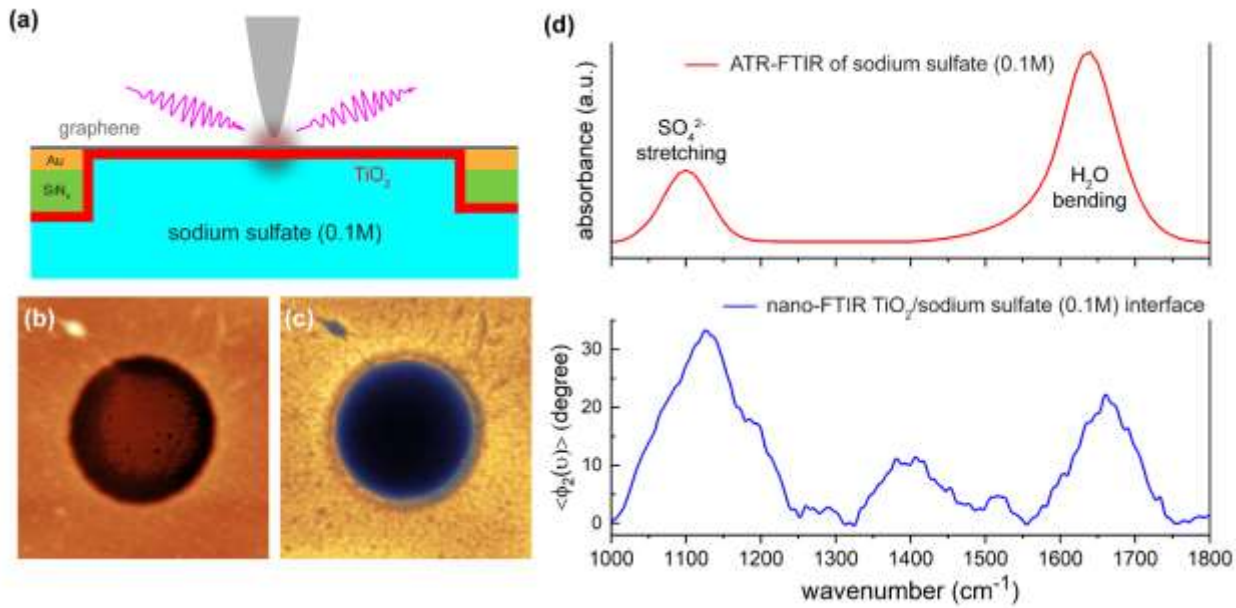

Figure 5 (a) Schematic of the plasmonically enhanced nano-FTIR experiment with the AFM tip situated over the metal oxide window closing the cell filled with liquid. Broadband synchrotron IR radiation is focused on the apex of the AFM tip, which enhances the electromagnetic field in the proximity of the apex in a range roughly equal to the tip radius (few nm) and scatters it to the far field. (b) Topography and (c) second harmonic optical amplitude images from the IR light scattered by the tip over the graphene/TiO_2 window covering a sodium sulfate aqueous solution (0.1 M) inside the cell. (d) Top: ATR-FTIR from a droplet of 0.1M sodium sulfate aqueous solution. Bottom: nano-FTIR of the 0.1M sodium sulfate solution acquired with the tip over the graphene/TiO_2 window (3nm thick)). The nano-FTIR spectrum is obtained from the phase of the scattered signal at the second harmonic of the cantilever oscillation frequency, which corresponds to the absorption coefficient of the material[42, 43, 47]. Notice the different amplitude of the bulk (ATR-FTIR) and nano-FTIR peaks of the SO_4^{2-} stretching, and water bending modes, and the presence of additional peaks between these two, visible only in the near surface region detected by nano-FTIR, showing the influence of the electrode composition in the structure of the electrical double layer.

In summary, we have shown that mechanically robust, free-standing, ultra-thin metal oxide membranes can be fabricated by PE-ALD on graphene and on polymer support materials. The oxide membranes are amorphous, uniform in thickness, and have compositions similar to those of the corresponding bulk oxides. Our proof-of-concept experiments show that they can be used as windows in environmental cells for XPS and nano-FTIR spectroscopic studies of gases (>1 bar) and of liquids near the interface. Their small thickness and good mechanical strength make them applicable to other electron/X-ray microscopy/spectroscopy or scanning probe techniques. By using different precursors and growing temperatures, a wide range of oxides of metals and semiconductors, including SiO_2, CoO_x, HfO_2, etc., could be fabricated and used as suspended ultra-thin films with different stoichiometry and crystallinity[26, 29, 48]. Therefore, we anticipate that the platform developed and presented here will open up new avenues for the study of catalytic, electrochemical, geochemical and other reactions at interfaces in practical conditions, as demonstrated by the results reported here. In addition, the ALD technique can also be used to grow membranes of other practical materials, such as nitrides, sulfides, noble metals, and 2D materials[26, 29, 48, 49]. Besides the applications for chemical studies just mentioned, the physical properties of the ultra-thin metal oxides can vary substantially from those of their bulk counterparts, including their magnetic properties, electron conductivity, and others that will be explored in the future. In the device area, the subsequent deposition of periodic array structures with different dielectric constants could be an ideal platform for photonic crystals and may be useful for vibrational spectroscopies and bio-chemical sensors[50].

Methods

Characterization of metal oxide thin films

The characterization of the metal oxides films was performed by XPS, TEM, scanning Auger spectroscopy and AFM measurements. The XPS measurements were performed using K-Alpha Plus XPS/UPS analyzer from Thermo Fisher Scientific equipped with a monochromatic Al K_α X-ray source (1486.6 eV) and an ion gun (Ar^+ or Ar_{75}^+) in an ultra-high vacuum chamber. A flood gun was used during the measurements. TEM and EELS measurements were performed with a JEOL 2100-F 200 kV Field-Emission Analytical Transmission Electron Microscope at an electron energy of 200 kV. Scanning Auger spectroscopy measurements were performed with an Oxford/Omicron Nano-Auger system under ultra-high vacuum of 10^{-10} Torr. The size of the electron-beam spot was ~10 nm. AFM topography measurements were done using Cypher ES (Asylum Research) and Bruker Icon systems.

AFM Nanoindentation

The AFM nanoindentation was performed using Cypher ES (Asylum Research). The normal spring constant of the cantilever was calibrated using the Sader Method[51]. The indentation rate was around 0.2 μm s^{-1}. A topographic scan was acquired before the indentation and the tip was positioned at the center of the suspended membrane for indentation measurements.

In situ XPS and nano-FTIR measurements

In situ XPS measurements were performed using the APPES-II end station in beamline 11.0.2 of the Advanced Light Source, at the Lawrence Berkeley National Laboratory. A differentially pumped analyzer (Phoibos 150, SPECS GmbH) equipped with three differentially pumped electrostatic lenses was used[52]. The design of the gas cell can be found elsewhere[21].

Nano-FTIR measurements were performed at beamline 2.4 of the Advanced Light Source, at the Lawrence Berkeley National Laboratory. The infrared light was focused onto the apex of a Pt

coated AFM tip in a neaSNOM (Neaspec, Germany) system. Tapping-mode operation was performed at the fundamental resonance frequency of the cantilever (250-350 kHz) with a free oscillation amplitude ranging from 70 to 90 nm and an amplitude setpoint of ~80%. The scattered near-field signal is retrieved by a lock-in amplifier tuned to the second and higher harmonics of the cantilever oscillation to eliminate the far field non-local scattered background. The complex-valued near-field spectrum is derived from a Fourier transform of the interferogram. The Fourier components are presented as real spectral amplitude "A" and phase "∅", normalized to reference spectra obtained with the tip outside the hole: $A_i(v) = A_i^{\text{sample}}(v)/A_i^{\text{reference}}(v)$ and $\emptyset_i(v) = \emptyset_i^{\text{sample}}(v) - \emptyset_i^{\text{reference}}(v)$ where v is the wavenumber. Reference spectra were taken on samples with flat spectral responses, either Au-coated Si or graphene on the Au-coated SiN membrane. The phase ∅ contains the absorption coefficient of materials and has been shown to be in good agreement with traditional FTIR absorption measurements[42, 43, 47].

Corresponding Author

*Email: mbsalmeron@lbl.gov (M.S.)

Author Contributions

[#]These authors contributed equally to this work.

Notes

The authors declare no competing financial interest.

ACKNOWLEDGMENT

We are grateful to Ed Wong of the Molecular Foundry for assistance in fabricating the gas cell. This work was supported by the Office of Basic Energy Sciences (BES), Division of Materials Sciences and Engineering, of the U.S. Department of Energy (DOE) under Contract DE-AC02-05CH11231, through the Structure and Dynamics of Materials Interfaces program (FWP KC31SM). Work was performed at the Molecular Foundry and at the Advanced Light Source user facilities, supported by the DOE Office of Basic Energy Sciences under the same contract number. X.Z was supported by a NSF-BSF grant number 1906014. C.M thanks the MEDC for a FPU fellowship grant (FPU14/02020).

REFERENCES

1. Putnis, C. V.; Ruiz-Agudo, E., The Mineral-Water Interface: Where Minerals React with the Environment. *Elements* **2013,** *9* (3), 177-182.
2. Brown, G. E.; Henrich, V. E.; Casey, W. H.; Clark, D. L.; Eggleston, C.; Felmy, A.; Goodman, D. W.; Gratzel, M.; Maciel, G.; McCarthy, M. I.; Nealson, K. H.; Sverjensky, D. A.; Toney, M. F.; Zachara, J. M., Metal oxide surfaces and their interactions with aqueous solutions and microbial organisms. *Chem Rev* **1999,** *99* (1), 77-174.
3. Al-Abadleh, H. A.; Grassian, V. H., Oxide surfaces as environmental interfaces. *Surf Sci Rep* **2003,** *52* (3-4), 63-161.
4. Zhao, Y.; Li, X. F.; Yan, B.; Xiong, D. B.; Li, D. J.; Lawes, S.; Sun, X. L., Recent Developments and Understanding of Novel Mixed Transition-Metal Oxides as Anodes in Lithium Ion Batteries. *Adv Energy Mater* **2016,** *6* (8).
5. Wu, Y., Metal oxides in energy technologies. In *Metal oxides series* [Online] First edition ed.; Elsevier,: London, 2018; p. 1 online resource. ScienceDirect. Restricted to UCB, UCD, UCI, UCLA, UCM, UCR, UCSC, UCSD, and UCSF http://uclibs.org/PID/329095.
6. Dey, A., Semiconductor metal oxide gas sensors: A review. *Mater Sci Eng B-Adv* **2018,** *229*, 206-217.
7. Jackson, S. D.; Hargreaves, J. S. J., *Metal oxide catalysis*. Wiley - VCH: Weinheim, 2008.
8. Somorjai, G. A.; Li, Y., *Introduction to surface chemistry and catalysis*. 2nd ed.; Wiley: Hoboken, N.J., 2010; p xii, 771 p.
9. de Jonge, N.; Ross, F. M., Electron microscopy of specimens in liquid. *Nat Nanotechnol* **2011,** *6* (11), 695-704.
10. Velasco-Velez, J. J.; Wu, C. H.; Pascal, T. A.; Wan, L. W. F.; Guo, J. H.; Prendergast, D.; Salmeron, M., The structure of interfacial water on gold electrodes studied by x-ray absorption spectroscopy. *Science* **2014,** *346* (6211), 831-834.
11. Hatty, V.; Kahn, H.; Heuer, A. H., Fracture toughness, fracture strength, and stress corrosion cracking of silicon dioxide thin films. *J Microelectromech S* **2008,** *17* (4), 943-947.

12. Striemer, C. C.; Gaborski, T. R.; McGrath, J. L.; Fauchet, P. M., Charge- and size-based separation of macromolecules using ultrathin silicon membranes. *Nature* **2007,** *445* (7129), 749-753.
13. Daulton, T. L.; Little, B. J.; Lowe, K.; Jones-Meehan, J., In situ environmental cell-transmission electron microscopy study of microbial reduction of chromium(VI) using electron energy loss spectroscopy. *Microsc Microanal* **2001,** *7* (6), 470-485.
14. Yuk, J. M.; Park, J.; Ercius, P.; Kim, K.; Hellebusch, D. J.; Crommie, M. F.; Lee, J. Y.; Zettl, A.; Alivisatos, A. P., High-Resolution EM of Colloidal Nanocrystal Growth Using Graphene Liquid Cells. *Science* **2012,** *336* (6077), 61-64.
15. Lee, C.; Wei, X. D.; Kysar, J. W.; Hone, J., Measurement of the elastic properties and intrinsic strength of monolayer graphene. *Science* **2008,** *321* (5887), 385-388.
16. Bunch, J. S.; Verbridge, S. S.; Alden, J. S.; van der Zande, A. M.; Parpia, J. M.; Craighead, H. G.; McEuen, P. L., Impermeable atomic membranes from graphene sheets. *Nano Lett* **2008,** *8* (8), 2458-2462.
17. Yulaev, A.; Guo, H. X.; Strelcov, E.; Chen, L.; Vlassiouk, I.; Kolmakov, A., Graphene Microcapsule Arrays for Combinatorial Electron Microscopy and Spectroscopy in Liquids. *Acs Appl Mater Inter* **2017,** *9* (31), 26492-26502.
18. Kolmakov, A.; Dikin, D. A.; Cote, L. J.; Huang, J. X.; Abyaneh, M. K.; Amati, M.; Gregoratti, L.; Gunther, S.; Kiskinova, M., Graphene oxide windows for in situ environmental cell photoelectron spectroscopy. *Nat Nanotechnol* **2011,** *6* (10), 651-657.
19. Velasco-Velez, J. J.; Pfeifer, V.; Havecker, M.; Weatherup, R. S.; Arrigo, R.; Chuang, C. H.; Stotz, E.; Weinberg, G.; Salmeron, M.; Schlogl, R.; Knop-Gericke, A., Photoelectron Spectroscopy at the Graphene-Liquid Interface Reveals the Electronic Structure of an Electrodeposited Cobalt/Graphene Electrocatalyst. *Angew Chem Int Edit* **2015,** *54* (48), 14554-14558.
20. Guo, H. X.; Strelcov, E.; Yulaev, A.; Wang, J.; Appathurai, N.; Urquhart, S.; Vinson, J.; Sahu, S.; Zwolak, M.; Kolmakov, A., Enabling Photoemission Electron Microscopy in Liquids via Graphene-Capped Microchannel Arrays. *Nano Lett* **2017,** *17* (2), 1034-1041.
21. Weatherup, R. S.; Eren, B.; Hao, Y. B.; Bluhm, H.; Salmeron, M. B., Graphene Membranes for Atmospheric Pressure Photoelectron Spectroscopy. *J Phys Chem Lett* **2016,** *7* (9), 1622-1627.
22. Lu, Y. H.; Larson, J. M.; Baskin, A.; Zhao, X.; Ashby, P. D.; Prendergast, D.; Bechtel, H. A.; Kostecki, R.; Salmeron, M., Infrared Nanospectroscopy at the Graphene-Electrolyte Interface. *Nano Lett* **2019,** *19* (8), 5388-5393.
23. Wang, L. D.; Travis, J. J.; Cavanagh, A. S.; Liu, X. H.; Koenig, S. P.; Huang, P. Y.; George, S. M.; Bunch, J. S., Ultrathin Oxide Films by Atomic Layer Deposition on Graphene. *Nano Lett* **2012,** *12* (7), 3706-3710.
24. Cao, C. H.; Mukherjee, S.; Liu, J.; Wang, B. Q.; Amirmaleki, M.; Lu, Z. L.; Howe, J. Y.; Perovic, D.; Sun, X. L.; Singh, C. V.; Sun, Y.; Filleter, T., Role of graphene in enhancing the mechanical properties of TiO2/graphene heterostructures. *Nanoscale* **2017,** *9* (32), 11678-11684.
25. Munther, M.; Shaygan, M.; Centeno, A.; Neumaier, D.; Zurutuza, A.; Momeni, K.; Davami, K., Probing the mechanical properties of vertically-stacked ultrathin graphene/Al2O3 heterostructures. *Nanotechnology* **2019,** *30* (18).
26. George, S. M., Atomic Layer Deposition: An Overview. *Chem Rev* **2010,** *110* (1), 111-131.

27. Singh, S.; Mahalingam, H.; Singh, P. K., Polymer-supported titanium dioxide photocatalysts for environmental remediation: A review. *Appl Catal a-Gen* **2013,** *462*, 178-195.
28. Egerton, R. F., *Electron energy-loss spectroscopy in the electron microscope*. 3rd ed.; Springer: Berlin ; New York, 2011; p xii, 491 p.
29. Profijt, H. B.; Potts, S. E.; van de Sanden, M. C. M.; Kessels, W. M. M., Plasma-Assisted Atomic Layer Deposition: Basics, Opportunities, and Challenges. *J Vac Sci Technol A* **2011,** *29* (5).
30. Gosset, L. G.; Damlencourt, J. F.; Renault, O.; Rouchon, D.; Holliger, P.; Ermolieff, A.; Trimaille, I.; Ganem, J. J.; Martin, F.; Semeria, M. N., Interface and material characterization of thin Al2O3 layers deposited by ALD using TMA/H2O. *J Non-Cryst Solids* **2002,** *303* (1), 17-23.
31. Haeberle, J.; Henkel, K.; Gargouri, H.; Naumann, F.; Gruska, B.; Arens, M.; Tallarida, M.; Schmeisser, D., Ellipsometry and XPS comparative studies of thermal and plasma enhanced atomic layer deposited Al2O3-films. *Beilstein J Nanotech* **2013,** *4*, 732-742.
32. Simpson, R.; White, R. G.; Watts, J. F.; Baker, M. A., XPS investigation of monatomic and cluster argon ion sputtering of tantalum pentoxide. *Appl Surf Sci* **2017,** *405*, 79-87.
33. Ring, E. A.; Peckys, D. B.; Dukes, M. J.; Baudoin, J. P.; de Jonge, N., Silicon nitride windows for electron microscopy of whole cells. *Journal of Microscopy* **2011,** *243* (3), 273-283.
34. Guo, J. H.; Luo, Y.; Augustsson, A.; Rubensson, J. E.; Sathe, C.; Agren, H.; Siegbahn, H.; Nordgren, J., X-ray emission spectroscopy of hydrogen bonding and electronic structure of liquid water. *Phys Rev Lett* **2002,** *89* (13).
35. Fuchs, O.; Maier, F.; Weinhardt, L.; Weigand, M.; Blum, M.; Zharnikovc, M.; Denlinger, J.; Grunze, M.; Heske, C.; Umbach, E., A liquid flow cell to study the electronic structure of liquids with soft X-rays. *Nucl Instrum Meth A* **2008,** *585* (3), 172-177.
36. Hedman, J.; Heden, P. F.; Nordling, C.; Siegbahn, K., Energy Splitting of Core Electron Levels in Paramagnetic Molecules. *Phys Lett A* **1969,** *A 29* (4), 178-&.
37. Avval, T. G.; Chatterjee, S.; Hodges, G. T.; Bahr, S.; Dietrich, P.; Meyer, M.; Thissen, A.; Linford, M. R., Oxygen gas, O-2(g), by near-ambient pressure XPS. *Surf Sci Spectra* **2019,** *26* (1).
38. Zaera, F., Probing Liquid/Solid Interfaces at the Molecular Level. *Chem Rev* **2012,** *112* (5), 2920-2986.
39. Zaera, F., New advances in the use of infrared absorption spectroscopy for the characterization of heterogeneous catalytic reactions. *Chem Soc Rev* **2014,** *43* (22), 7624-7663.
40. Campion, A.; Kambhampati, P., Surface-enhanced Raman scattering. *Chem Soc Rev* **1998,** *27* (4), 241-250.
41. Shen, Y. R.; Ostroverkhov, V., Sum-frequency vibrational spectroscopy on water interfaces: Polar orientation of water molecules at interfaces. *Chem Rev* **2006,** *106* (4), 1140-1154.
42. Bechtel, H. A.; Muller, E. A.; Olmon, R. L.; Martin, M. C.; Raschke, M. B., Ultrabroadband infrared nanospectroscopic imaging. *P Natl Acad Sci USA* **2014,** *111* (20), 7191-7196.
43. Centrone, A., Infrared Imaging and Spectroscopy Beyond the Diffraction Limit. *Annu Rev Anal Chem* **2015,** *8*, 101-126.
44. Muller, E. A.; Pollard, B.; Bechtel, H. A.; van Blerkom, P.; Raschke, M. B., Infrared vibrational nano-crystallography and nano-imaging. *Sci Adv* **2016,** *2* (10).

45. Baskin, A.; Prendergast, D., "Ion Solvation Spectra": Free Energy Analysis of Solvation Structures of Multivalent Cations in Aprotic Solvents. *J Phys Chem Lett* **2019,** *10* (17), 4920-4928.
46. Baskin, A.; Prendergast, D., Exploring chemical speciation at electrified interfaces using detailed continuum models. *J Chem Phys* **2019,** *150* (4).
47. Huth, F.; Govyadinov, A.; Amarie, S.; Nuansing, W.; Keilmann, F.; Hilenbrand, R., Nano-FTIR Absorption Spectroscopy of Molecular Fingerprints at 20 nm Spatial Resolution. *Nano Lett* **2012,** *12* (8), 3973-3978.
48. Oviroh, P. O.; Akbarzadeh, R.; Pan, D. Q.; Coetzee, R. A. M.; Jen, T. C., New development of atomic layer deposition: processes, methods and applications. *Sci Technol Adv Mat* **2019,** *20* (1), 465-496.
49. Hao, W.; Marichy, C.; Journet, C., Atomic layer deposition of stable 2D materials. *2d Mater* **2019,** *6* (1).
50. Akahane, Y.; Asano, T.; Song, B. S.; Noda, S., High-Q photonic nanocavity in a two-dimensional photonic crystal. *Nature* **2003,** *425* (6961), 944-947.
51. Sader, J. E.; Chon, J. W. M.; Mulvaney, P., Calibration of rectangular atomic force microscope cantilevers. *Rev Sci Instrum* **1999,** *70* (10), 3967-3969.
52. Bluhm, H.; Andersson, K.; Araki, T.; Benzerara, K.; Brown, G. E.; Dynes, J. J.; Ghosal, S.; Gilles, M. K.; Hansen, H. C.; Hemminger, J. C.; Hitchcock, A. P.; Ketteler, G.; Kilcoyne, A. L. D.; Kneedler, E.; Lawrence, J. R.; Leppard, G. G.; Majzlan, J.; Mun, B. S.; Myneni, S. C. B.; Nilsson, A.; Ogasawara, H.; Ogletree, D. F.; Pecher, K.; Salmeron, M.; Shuh, D. K.; Tonner, B.; Tyliszczak, T.; Warwick, T.; Yoon, T. H., Soft X-ray microscopy and spectroscopy at the molecular environmental science beamline at the Advanced Light Source. *J Electron Spectrosc* **2006,** *150* (2-3), 86-104.

Supporting Information for Ultra-thin Free-Standing Oxide Membranes for Electron and Photon Spectroscopy Studies of solid-gas and solid-liquid interfaces

Yi-Hsien Lu [†,#], Carlos Morales [†,‡,#], Xiao Zhao [†,§,#], Matthijs van Spronsen [†], Artem Baskin [//], David Prendergast [//], Peidong Yang [†,Δ], Hans A. Bechtel [⊥], Edward Barnard [//], Frank Ogletree [//], Virginia Altoe [//], Leonardo Soriano [‡], Adam Schwartzberg [//] and Miquel Salmeron [†,§,]*

[†] Materials Sciences Division, Lawrence Berkeley National Laboratory, Berkeley, California, 94720, United States

[//] Molecular Foundry, Lawrence Berkeley National Laboratory, Berkeley, California, 94720, United States

[§]Department of Materials Science and Engineering, University of California at Berkeley, Berkeley, California 94720, United States

[Δ] Department of Chemistry, University of California, Berkeley, California, 94720, United States

[‡]Departamento de Física Aplicada and Instituto de Ciencia de Materiales Nicolás Cabrera, Universidad Autónoma de Madrid, Cantoblanco, 28049 Madrid, Spain

[⊥]Advanced Light Source, Lawrence Berkeley National Laboratory, Berkeley, California, 94720, United States

PE-ALD Growth of Metal Oxides

The Al_2O_3 and TiO_2 metal oxides were grown on graphene and on polymers, e.g. Formvar and PMMA (polymethyl methacrylate) by plasma-enhanced atomic layer deposition (PE-ALD, Oxford Instruments FlexAl and Cambridge Fiji F200 systems). In addition to O_2, trimethylaluminium ($Al_2(CH_3)_6$, TMA) and tetrakis(dimethylamino)titanium ($Ti[N(CH_3)_2]_4$, TDMAT) were used as precursors for Al_2O_3 and TiO_2, respectively. In the Oxford FlexAl system, a turbomolecular pump was used to maintain a base pressure of 10^{-6} Torr inside the reactor before deposition. The gas-delivery line was kept at 100°C, and the substrate was heated to 40-120°C during deposition. In the Cambridge Fiji F200 system, N_2 was used as the carrier gas, the gas delivery line was heated to 150 °C, and the chamber kept at 100 °C during the deposition process. A sample holder was specially designed to prevent PE-ALD coating of both sides of the graphene or polymers (Figure S1). The holder consists of a flat stainless-steel clamp with a circular hole fixed on top of the graphene/polymer capped SiN membrane sitting on a Si chip. The perforated region is located on a circular hole for the PE-ALD growth.

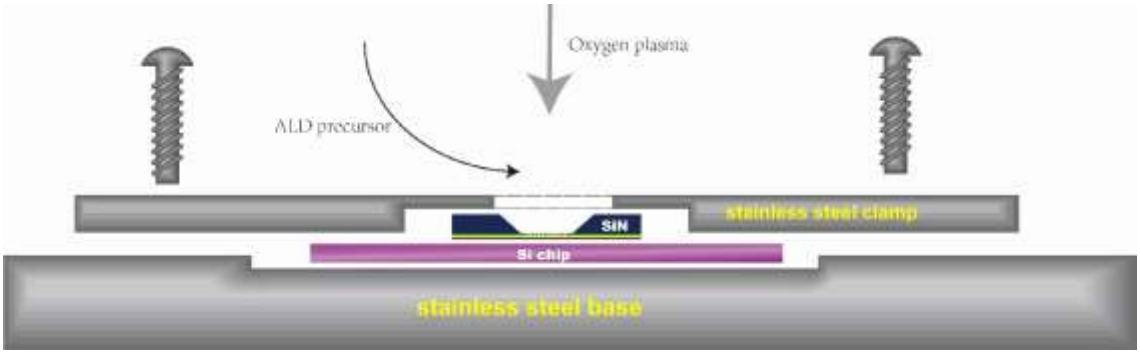

Figure S1 Design of the sample holder for PE-ALD. A flat stainless-steel clamp with a circular hole is fixed on top of the graphene or polymer capped perforated SiN membrane sitting on a Si chip. The perforated SiN region is located on a circular hole for PE-ALD growth. Such design avoids deposition of the metal oxide on the back side of SiN membrane (lying over the Si chip).

The thickness or growth rate of metal oxides was measured by ellipsometry directly deposited on silicon substrates. AFM step measurements were also performed to confirm the accuracy. In order to understand if there is deviation in growth rate using suspended graphene as a support, EELS measurement was performed on an Al_2O_3/graphene membrane, as shown in Figure S2.

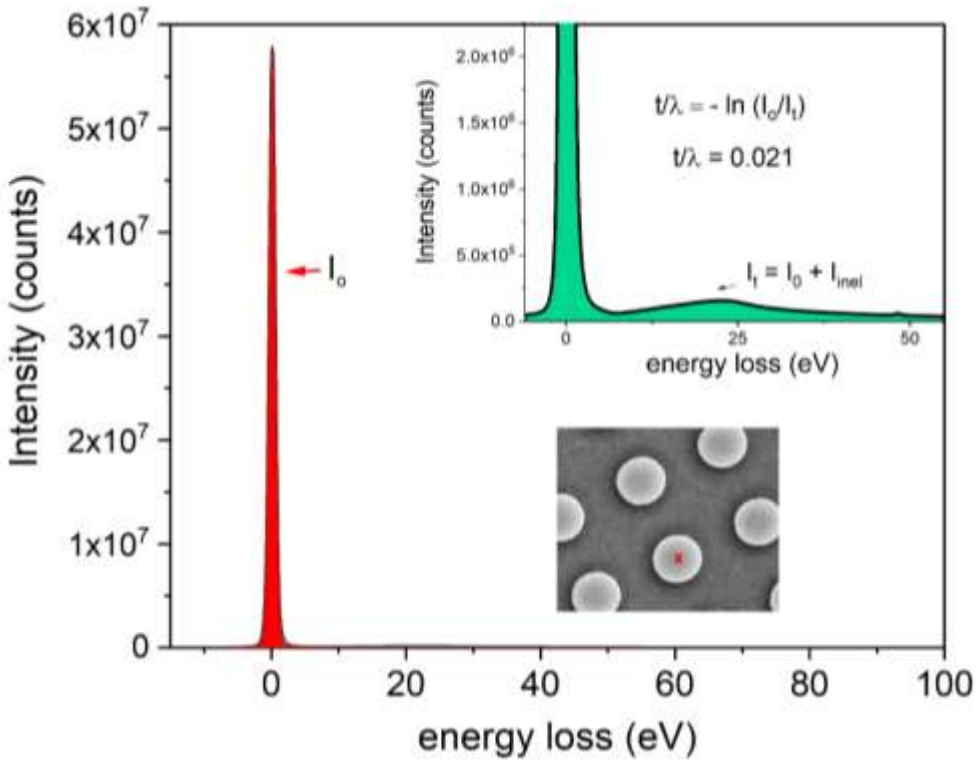

Figure S2 EELS spectrum on an intact Al_2O_3/graphene window. Based on the ellipsometry data measured on a Si substrate, the growth rate of Al_2O_3 at 40 °C (FlexAl, Oxford Instruments) is 7 cycles/nm. The window showing here (TEM image shown in the bottom inset) was grown with 20 cycles. To estimate the thickness, one can use log-ratio method, comparing the area under I_0 (zero loss, inelastic peak; shown as red shaded region) with I_t (total area under the whole spectrum; shown as green shaded region in the right top inset)[1]. The thickness is given by $t/\lambda = \ln(I_t/I_0)$. Here, the measurement was performed under 200 keV, corresponding to the inelastic mean free path of ~ 140 nm[2]. From the above equation, the estimated thickness of the window is ~ 2.95 nm (including ~ 0.3 nm graphene), which is close to the expected value (3.15 nm). Therefore, the ellipsometry data obtained on Si substrates can also be applied to the case of using suspended graphene as a support.

Graphene and polymer transfer on perforated SiN membranes

Commercial single-layer graphene grown on Cu foil (Graphene Supermarket or Sigma-Aldrich) by chemical vapor deposition (CVD) was used as base material. The graphene on one side of the foil was removed by O_2 plasma. An adhesive Al foil frame window was stuck to the untreated side and then floated on a Cu etchant solution (~0.2 M sodium persulfate)[3]. After etching away the Cu, graphene along with the Al window frame, was transferred to a deionized water reservoir (~500 ml) to remove the salt residue. The transfer process to the water reservoir was repeated twice to ensure complete salt removal. A Cr (2 nm)/Au (10-30 nm) coated SiN membrane (50 or 200 nm thickness) perforated with an array of 1000 nm or 500 nm circular holes (Norcada) was placed in the reservoir underneath the graphene and carefully lifted up from the air/water interface to conclude the graphene transfer.

Polymers were also be used as a support of the PE-ALD grown metal oxides. These included poly(methyl methacrylate) (PMMA, Microchem) or polyvinyl formal (Formvar, Electron Microscopy Sciences). These polymers can be transferred onto the Cr/Au coated perforated SiN membranes by spin-coating and removed later with acetone. Formvar can also be transferred by soaking a glass microscope slide into the Formvar solution (1,2-dichloroethane) and subsequently immersing the glass slide in water slowly. Then, floating Formvar layers are lifted by the Au coated SiN TEM grids. The Formvar polymer can later be dissolved in chloroform.

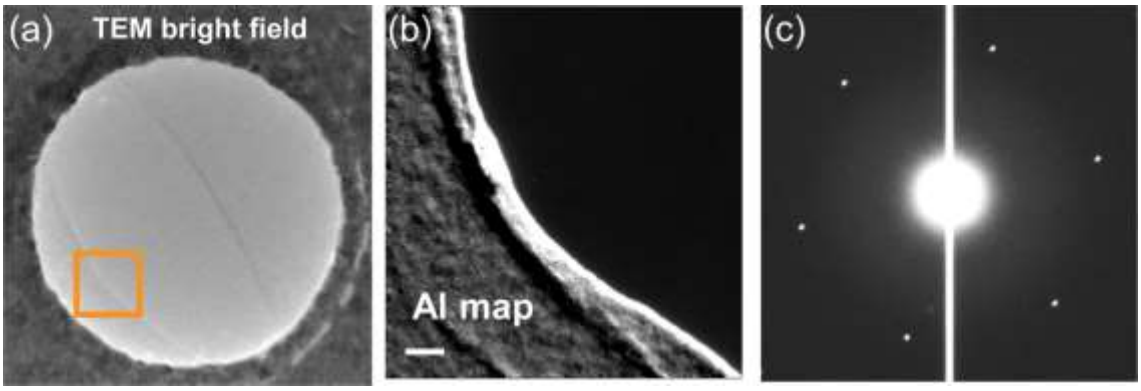

Figure S3 (a) TEM bright field image on a ruptured Al_2O_3/graphene window. (b) Corresponding EELS (Al-$L_{2,3}$ edge) map from a region containing the edge of the ruptured hole in (a) (orange rectangle). (c) A selected electron diffraction pattern from an intact region showing the hexagonal symmetry pattern from graphene, with the amorphous oxide contributing only the background.

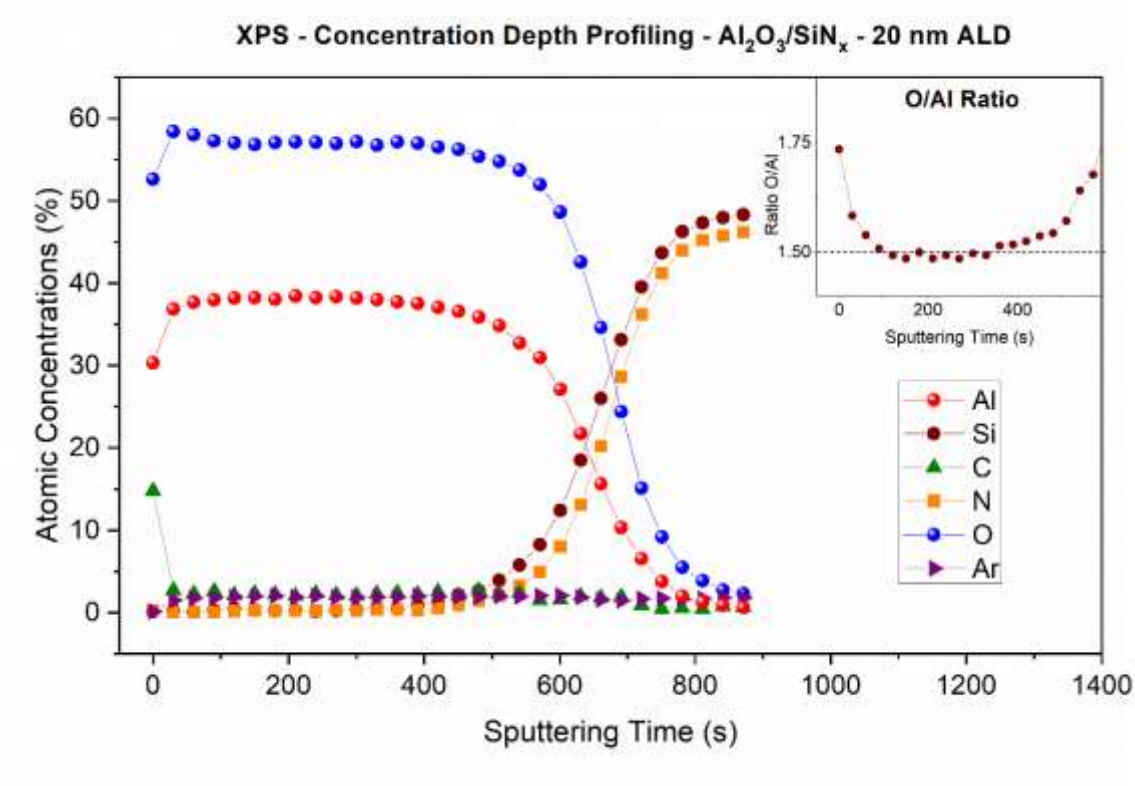

Figure S4 Depth profile XPS measurements of a 20 nm Al_2O_3 thin film grown by PE-ALD on a SiN substrate. XPS measurements were performed by K-Alpha Plus XPS/UPS analyzer (Thermo Fisher Scientific) equipped with a monochromatic Al Kα X-ray source (1486.6 eV) and an ion

gun in an ultrahigh vacuum chamber (base pressure ~10^{-10} mbar). Depth profile composition of the Al_2O_3 film from XPS peak intensities. Each point corresponds to an additional 30 seconds of sputtering. Sputtering by monoatomic Ar^+ ions of 2000 eV. Top right inset shows the O/Al ratio of the total O1s and Al 2p intensities. The depth profile study confirms the O/Al stoichiometric ratio of ~ 1.5 in the bulk.

Ar_{75}^+ clusters Sputtering time (s)	**Atm. Con. C (%)**	**Atm. Con. Al (%)**	**Atm. Con. O (%)**	**O/Al**
0	**15.7 (±1)**	**32.4 (±1.6)**	**51.9 (±2.5)**	**1.6**
30	**1.1 (±0.5)**	**41.2 (±2.1)**	**57.7 (±2.8)**	**1.4**

Table S1 A gentle sputtering with Ar_{75}^+ clusters at 8000 eV eliminates carbon excess. Besides, the O/Al ratio decreases to a value next to stoichiometric 1.5. Unlike monoatomic Ar^+, Ar clusters sputtering do not result in Ar implantation into the metal oxide matrix.

References

1. Egerton, R. F., *Electron energy-loss spectroscopy in the electron microscope*. 3rd ed.; Springer: Berlin ; New York, 2011; p xii, 491 p.
2. Iakoubovskii, K.; Mitsuishi, K.; Nakayama, Y.; Furuya, K., Mean free path of inelastic electron scattering in elemental solids and oxides using transmission electron microscopy: Atomic number dependent oscillatory behavior. *Phys Rev B* **2008,** *77* (10).
3. Weatherup, R. S.; Eren, B.; Hao, Y. B.; Bluhm, H.; Salmeron, M. B., Graphene Membranes for Atmospheric Pressure Photoelectron Spectroscopy. *J Phys Chem Lett* **2016,** *7* (9), 1622-1627.